Dynamic Nuclear Polarization and Potential Applications to Medicine Imaging

Ryan Zielinski
University of New Hampshire
rbziel@jlab.org

May 9, 2014

Abstract

Using Dynamic Nuclear Polarization (DNP) it is possible to create a nuclear polarization that is many orders of magnitude larger than the corresponding thermal equilibrium polarization. This is particularly useful in medical imaging, where larger polarizations correspond to increases in the signal to noise ratio of traditional MRI. An increase in sensitivity, driven by DNP, provides researches access to new nuclei for MR imaging, and the new nuclei can be chosen to target specific processes in the human body. One example is carbon-13, which can be used to image the catalysis of ^{13}C-pyruvate to ^{13}C-lactate in cancerous tissue. Early research has shown a correlation between a tumor's treatment response and this catalysis rate. Researchers have achieved carbon-13 polarizations of 42%, which represents a 40,000 fold enhancement over the thermal equilibrium polarization.

1 Introduction

Nuclear Magnetic Resonance (NMR) spectroscopy and Magnetic Resonance Imaging (MRI) have, historically, been the main methods for non-invasive medical imaging. The implementation of these procedures relies on the ability to polarize the material being imaged. The sensitivity of the imaging analysis is proportional to the level of polarization, where the polarization is defined as the fractional difference between nuclear spins aligned with and against an applied magnetic field. This spin polarization is proportional to the magnetic moment of the nuclei and applied magnetic field and inversely proportional to the temperature. Field strengths are typically on the order of a few Tesla [1].

Current MRI techniques use a large magnetic field to polarize hydrogen atoms (protons) found in the human body, relying on the high concentration of protons in water and fat to overcome poor polarization [2]. The small magnetic moment of the proton results in a magnetic energy that is much less than the proton's thermal energy at room temperature and creates a very low level of polarization. Even at the applied magnetic fields of 21 T used in high-resolution NMR (an order of magnitude higher than the field strength used in clinical MRI) the proton polarization is only 0.007% [3].

Small equilibrium polarizations can be enhanced through Dynamic Nuclear Polarization (DNP). The large magnetic moment of the electron leads to a comparatively large polarization. DNP transfers this large electron polarization to nuclear polarization. The polarization is driven using microwave transitions, with samples kept at roughly 1 K in a multi-Tesla magnetic field. Nuclear polarization (also referred to as hyperpolarization) can approach 100% through the DNP mechanism, resulting in a greater than 10,000 fold increase in MRI signal compared to the equilibrium case [4]. This allows for the imaging of nuclei that were previously excluded due to their low natural abundance and small equilibrium polarizations.

1.1 Thermal Equilibrium Polarization

At large magnetic fields and low temperatures, nuclei with a non-zero magnetic moment (μ) tend to align themselves with the field. The Zeeman interaction (see Figure 1) separates the nuclei into spin-dependent energy states. There are two such states for spin-$\frac{1}{2}$ nuclei, and the corresponding Zeeman energy is $\pm\mu \cdot B$. The vector polarization is defined as the difference in the fraction of nuclei aligned with and against an applied magnetic field such

that

$$P = \frac{N^{\uparrow} - N^{\downarrow}}{N^{\uparrow} + N^{\downarrow}}, \tag{1}$$

where $N^{\uparrow}$ is the number of states aligned with the field and $N^{\downarrow}$ is the number of states anti-aligned with the field.

The relative state populations can be expressed using Boltzmann statistics [5] as

$$\frac{N_1}{N_2} = \exp\left(\frac{-\Delta E}{k_B T}\right) = \frac{N^{\uparrow}}{N^{\downarrow}} = \exp\left(\frac{2\mu B}{k_B T}\right), \tag{2}$$

where k_B is the Boltzmann constant and T is the temperature. Combining equations (1) and (2) leads to an expression for the thermal equilibrium polarization

$$P_{\mathrm{TE}} = \frac{e^{\frac{\mu B}{k_B T}} - e^{\frac{-\mu B}{k_B T}}}{e^{\frac{\mu B}{k_B T}} + e^{\frac{-\mu B}{k_B T}}}. \tag{3}$$

At 5 T and 1 K, this thermal equilibrium polarization is 99.8% [6] for an electron but less than 1% for a proton ($\mu_p \approx \frac{\mu_e}{660}$). Another example of a spin-$\frac{1}{2}$ nuclei is carbon-13, which, at the same field strength and temperature, has a thermal equilibrium polarization of 0.001%. A extensive list of the magnetic moments of nuclei is found in [7].

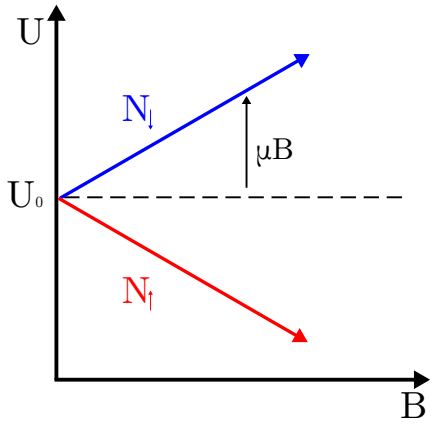

Figure 1: Zeeman splitting of a spin-$\frac{1}{2}$ particle of magnetic moment μ in a magnetic field B.

1.2 The DNP Process: Solid-State Effect

Using the proton as an example, a simple description of the solid-state effect and DNP process can be given as follows: The solid target material sample, containing a large of number of polarizable protons, is doped with paramagnetic radicals to provide uniformly distributed,

unpaired electron spins throughout the sample. A strong magnetic field (between 2 T and 5 T) is applied at low temperature (less than 4 K) to create a large thermal equilibrium polarization of the unpaired electrons. The spin-spin interaction in the magnetic field of the electron and proton causes hyperfine splitting and four distinct energy levels based upon the alignment of the proton and electron spins, as shown in Figure 2. The corresponding Hamiltonian is

$$H = \vec{\mu}_e \cdot \vec{B} + \vec{\mu}_p \cdot \vec{B} + H_{ss}, \tag{4}$$

where the first two terms are the Zeeman interaction of the electron and proton, respectively and H_{ss} is the spin-spin interaction term [8].

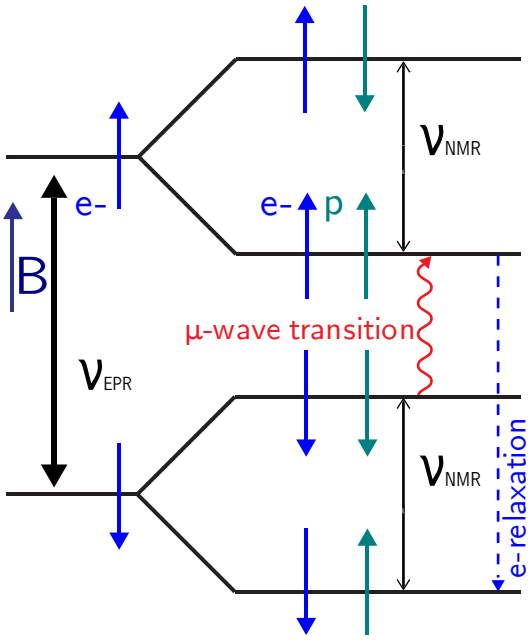

Figure 2: Microwaves transition a paired spin state, $e_\downarrow p_\downarrow \rightarrow e_\uparrow p_\uparrow$, to produce positive polarization. Based on a figure from [9].

Electron spins can be flipped by applying an RF-field at the electron paramagnetic resonance (EPR) frequency, ν_{EPR}, which corresponds to a Zeeman energy of $\vec{\mu}_e \cdot \vec{B}$. In a similar manner, the proton spin can be flipped with an RF-field at the nuclear magnetic resonance (NMR) frequency, ν_{NMR}, corresponding to a Zeeman energy of $\vec{\mu}_p \cdot \vec{B}$.

Traditional dipole selection rules forbid the simultaneous flipping of both spins, but the presence of the spin-spin interaction creates mixing between electron and proton states, allowing access to these previously forbidden transitions [10]. Microwaves tuned to the frequency $\nu_\mu = \nu_{\mathrm{EPR}} - \nu_{\mathrm{NMR}}$ (140.1 GHz at 5 T and 1 K) induce the transition $e_\downarrow p_\downarrow \rightarrow e_\uparrow p_\uparrow$.

The electrons tend to relax to the lower energy state, $e_\uparrow p_\uparrow \rightarrow e_\downarrow p_\uparrow$, in a few seconds, but the relaxation time of the proton is tens of minutes. This allows a single electron to polarize multiple protons, driving a positive proton polarization state. A negative proton polarization state is achieved by tuning the microwaves to the frequency $\nu_\mu = \nu_{\text{EPR}} + \nu_{\text{NMR}}$ (140.5 GHz at 5 T and 1 K).

1.3 Measuring Polarization in DNP: NMR Theory

The Zeeman interaction causes a particle with spin S to split into $2S + 1$ energy levels when placed in a magnetic field $\vec{B}$. Each level is split by the energy $h\omega_L = \vec{\mu}\cdot\vec{B}/S = g\mu_N B$, where g is g-factor for the particle of spin S and μ_N is the nuclear magneton. A RF-field applied at the Larmor frequency, ω_L, can flip the spin of the particle, as it absorbs or emits energy interacting with the field. The response of the polarized sample to the RF is characterized by its magnetic susceptibility and is a function of the RF-field frequency, ω,

$$\chi(\omega) = \chi'(\omega) - i\chi''(\omega), \tag{5}$$

where $\chi'(\omega)$ is the dispersive term and $\chi''(\omega)$ is the absorptive part of the susceptibility [9]. The absorptive term is proportional to the absolute polarization of the sample through the following integral relation [11]

$$P \propto \int_0^\infty \chi''(\omega)d\omega. \tag{6}$$

This absorptive term is measured by embedding a RF transmission coil in the polarized sample. The RF field is swept through the Larmor frequency, creating changes in the inductance of the coil as the sample absorbs and emits energy. Measuring this change gives access to the absorptive term [9]. The proportionality constant in equation (6) is found by comparing the NMR signal, in the absence of microwaves, to the calculated thermal equilibrium polarization, shown in equation (3).

1.4 Spin Relaxation and Polarization Decay

The vibrational and rotational motion of the proton and electron create a lattice structure within the sample [12]. Irradiating microwaves add spin energy to the proton-electron system in order to create polarization. The additional spin energy is in thermal contact with the lattice, which provides a mechanism for the electron or proton to "give up" its spin energy

gained through polarization. They can return to their respective thermal equilibrium states by emitting a lattice phonon [13]. This process is referred to as spin-lattice relaxation. The spin coupling strength to the lattice is proportional to the magnetic moment of the polarized spin and can explain the relatively shorter relaxation time of the electron ($\mu_e \approx 660\mu_p$).

The average lifetime of nuclei in the higher energy state is referred to as the relaxation time, T_1. This T_1 time can be used to estimate the polarization decay rate of a hyperpolarized sample after terminating the microwave irradiation and ceasing the polarizing spin transitions. Changes in temperature and field strength change the vibrational and rotational energy of the lattice, which has a direct impact on T_1. This is important for medical applications where it is not feasible to inject a patient with a 1 K DNP solid immersed in a 5 T field.

2 Experimental DNP Polarizer

An overview of a DNP polarizer [3, 4] used for medical imaging is shown in Figure 3. A highly-uniform superconducting solenoid (typical bore length [diameter] $\approx$ 40 [15] cm) provides the magnetic field and is kept in a liquid helium bath within the cryostat. Microwave frequency and power constraints limit the maximum DNP magnet field strength to 7 T. The cryostat itself is contained within an external vacuum vessel. To minimize liquid helium loss, the helium reservoir is kept in thermal contact with a liquid nitrogen shield. A system of roots pumps continually pump on the magnet space to lower the vapor pressure and thus temperature of the system. This allows temperatures to reach 1 K from the 4 K liquid helium boiling temperature. The vapor pressure is measured using the pressure transducer. Carbon resistors, which have a well defined response to temperature, are used to determine the liquid helium level. The resistors are fed into a feedback loop to continuously monitor this level.

The DNP insert is approximately a meter in length and is placed through the sample port into the cold bore of the magnet. Waveguides transport microwaves from the exterior RF source to the sample holder, which terminates in a metal container to confine the microwaves. Inside the metal container is a NMR coil to measure the polarization. Prior to loading the sample, the sample holder and sample cup are pre-cooled in a bath of liquid nitrogen. The frozen sample pellets are then placed into the cooled sample cup and both the holder and cup are lowered into the variable temperature insert. This design allows the sample to be

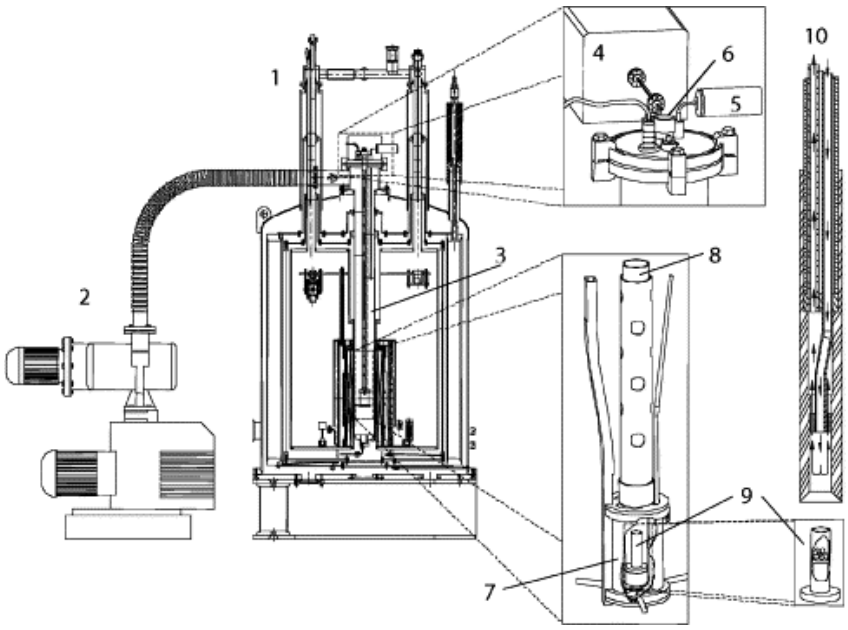

Figure 3: Experimental DNP setup. (1) DNP polarizer and cryostat (2) vacuum pump (3) variable temperature insert (4) microwave source (5) pressure transducer (6) sample port (7) microwave waveguide (8) sample holder (9) sample container (10) dissolution wand. Reproduced from [4].

removed from the bore for dissolution.

Dissolution is necessary to create a liquid solution (of the frozen sample) that is suitable for use in patients. Prior to dissolution, the microwave irradiation is stopped and the sample is raised above the liquid helium level, but it is still kept within the magnetic field. A syringe of boiling water is connected to the injection wand. The injection wand is docked with the sample cup through the sample holding tube. The hot water is rapidly injected into the sample holding tube, and the dissolved sample is displaced and collected through the injection wand's second tube.

3 Applications to Medical Imaging

The current method to detect a tumor's response to treatment is largely based on imaging measurements of the physical tumor size over time [14]. It may take weeks for these changes to manifest, and therefore an imagining technique with the ability to highlight early indications of the tumor's response could help predict a treatment's outcome in advance. One possibility is to look at the difference in cell metabolism between cancerous and healthy tissue. Traditional MRI is ideal for detecting this molecular specific information [15] but

lacks the sensitivity (polarization) to target metabolic processes. DNP can overcome these challenges, and extensive research has been carried out on hyperpolarized ^{13}C as an imaging agent.

3.1 Hyperpolarized Carbon-13

Sample polarization results from J. Wolber *et al.* [3] on ^{13}C-urea are shown in Figure 4. The measurements were performed at 3.354 T and 1.2 K, corresponding to a microwave frequency of $\approx$ 94 GHz. The authors used trityl radicals to dope the samples with unpaired electron spins and measured the effect dopant concentration had on the polarization and T_1. They achieved a maximum polarization of 42% (T_1 = 28200 s, measured at 3.354 T and 1.2 K), which represents a $\approx$ 40,000 enhancement over the thermal equilibrium polarization. Microwave power was kept constant at 100 mW. After dissolution they were able to achieve a 20% ^{13}C-urea polarization.

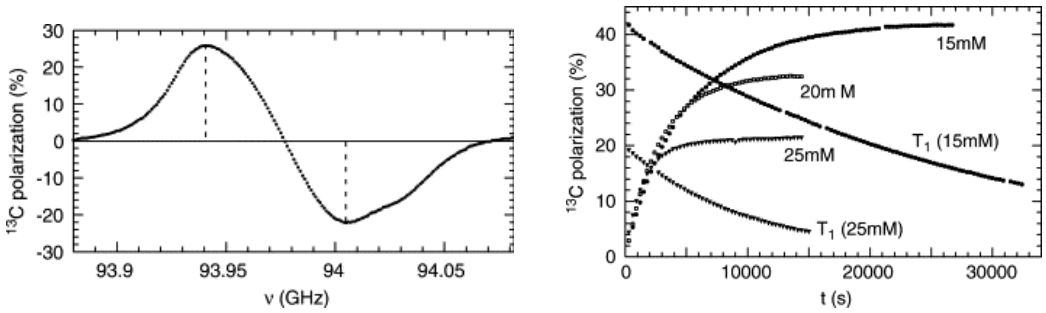

(a) (b)

Figure 4: ^{13}C hyper polarization: **(a)** positive (93.952 GHz, 26%) and negative (94.005 GHz, -22%) polarization states **(b)** effect of dopant (in millimolar) on maximum polarization and T_1. Reproduced from [3].

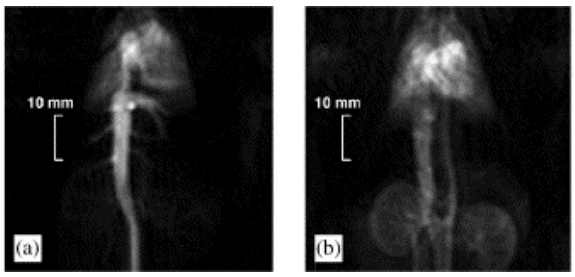

Figure 5: Polarized ^{13}C imaging of a rat. Reproduced from [3].

J. Wolber *et al.* [3] were subsequently able to MR image a rat using the hyperpolarized ^{13}C-urea solution. They injected the solution into the tail of a rat and could visualize the

heart, lungs and kidneys. Figure 5**(a)** shows the right side of the heart and the vascular structure of the lungs. The image was taken 1 s after injection. Figure 5**(b)** shows a more complete image of the heart and includes the kidneys. This image was taken 3 s after injection.

Cancer cells and tumors have higher rates of glucose consumption (glycolysis) and lactate production when compared with normal tissue [16]. The end product of glycolysis, pyruvate, can be catalyzed in the cell to produce lactate. ^{13}C-pyruvate is ideal for medical DNP because it is (1) easily polarized (2) non-toxic (3) has a relatively long T_1 relaxation time (4) is rapidly metabolized in the cell and (5) has a high concentration of polarized material after dissolution [2]. Jan H. Ardenkjaer-Larsen *et al.* [18] have demonstrated ^{13}C-pyruvate polarizations of 36% and 18% before and after dissolution, respectively.

Figure 6 shows clinical evidence of the ability to use the link between glycolysis and lactate production to assess tumor treatment. Sam E. Day *et al.* [14] injected hyperpolarized ^{13}C-pyruvate into lymphoma bearing mice and measured the lactate catalysis rate using MRI. They found a reduction in the catalysis rate in mice that received a drug treatment. Figure 6**(a)** shows a representative spectrum of the signal intensities of ^{13}C-lactate and ^{13}C-pyruvate prior to treatment. The solid lines are fit to a model describing the pyruvate-lactate conversion process. The decrease in signal is due to the decay in polarization and the group found a T_1 of $\sim$ 40 s. The first 15 s are the time it took to prepare and begin imaging the mouse. The tumor's response to the treatment is seen in Figure 6**(b)**, as a ratio between lactate and pyruvate signal intensities 20 hours after beginning treatment. The shaded regions are one standard-deviation from the mean and the black bar between 20-25 s is the time when imaging was performed.

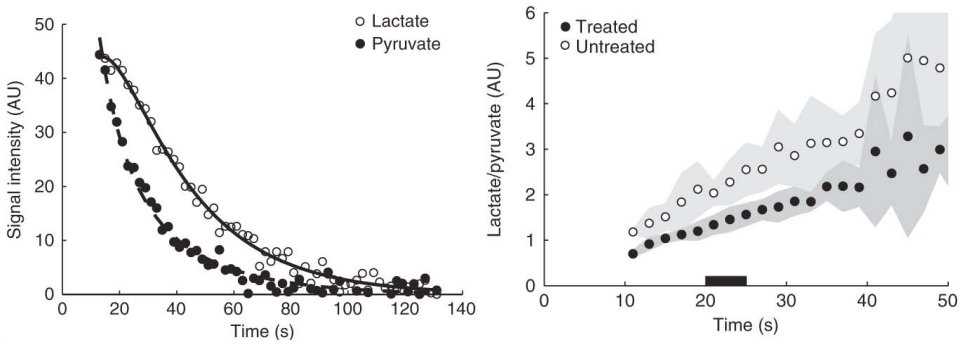

(a) (b)

Figure 6: Catalyis of hyperpolarized ^{13}C-pyruvate into ^{13}C-lactate in a treated and untreated tumor. AU is arbitrary units. Reproduced from [14].

4 Conclusion and Outlook

Enhancing nuclear polarizations using DNP has the potential to provide physicians with new ways to diagnose and treat diseases, but there are still technical challenges to overcome before DNP is viable for use in MRI on human subjects. The experimental apparatus described in Section 2 is not viable for clinical use because (1) open-handling of the sample is not sterile (2) using large amounts of liquid cryogens is expensive (3) polarization time is slow and (4) it can't polarize large quantities of material [18]. Jan H. Ardenkjaer-Larsen *et al.* [18] have developed a new polarizer that addresses these issues, but there are still the issues of quality control and automating the procedure.

The short room-temperature T_1 ($\sim$ 40 s) also presents limitations by placing strict time constraints on the imaging process. J. Wolber *et al.* [3] have showed that polarization build-time and decay can be changed by altering the concentration of the trityl radical dopant. It's possible that other dopants could have similar effects but also be more effective than trityl radicals. DNP has a long history in nuclear physics so there are a good number of known dopants. For example, L. Lumata *et al.* [19] investigated TEMPO (commonly used to dope ammonia for proton polarization) and found it less effective than trityl. Regardless, there are more than two possible dopants (and more than one polarizable nucleus) available, and it is still possible for improvements to be made.

In summary, using Dynamic Nuclear Polarization (DNP) it is possible to create nuclear polarizations that are significantly larger than the corresponding thermal equilibrium polarization. The DNP technique has been demonstrated on carbon-13 to produce an enhanced polarization that is 40,000 times larger than the thermal equilibrium polarization. This allows physicians to use the molecule specific imagining power of MRI to image specific biological pathways in the human body that would have otherwise been not possible due to the small abundance and polarization of the nuclei marking the pathway. While further research needs to be done before this is a viable clinical option, current research has already shown that hyperpolarized carbon-13 could be potentially used to asses cancer and tumor treatment.

References

[1] D. Marshall, Can. Assoc. Radiol. J. **45**(3), 180 (1994).

[2] J. Kurhanewicz *et al.*, Neoplasia, **13**(2), 81 (2011).

[3] J. Wolber *et al.*, Nucl. Instrum. Meth. **A526**, 173 (2004).

[4] J. H. Andrenkjaer-Larsen *et al.*, Proceedings of the National Academy of Sciences **100**(18), 10158 (2003).

[5] R. K. Pathria and Paul D. Beale, "Statistical Mechanics. 3rd ed," Elsevier, 2011. 53.

[6] T. D. Averett *et al.*, Nucl. Instrum. Meth. **A427**, 440 (1999).

[7] Gladys H. Fuller, J. Phys. Chem. Ref. Data **5**, 4 (1976).

[8] B. Corzilius, A. A. Smith and R. G. Griffin, J. Chem. Phys. **137**, 054201 (2012).

[9] D. G. Crabb and W. Meyer, Annual Review of Nuclear and Particle Science **47**, 67 (1997).

[10] A. Abragam and M. Goldman, Rep. Prog. Phys. **41**(3), 395 (1978).

[11] M. Goldman, Journal of Magnetic Resonance **17**(3), 393 (1975).

[12] Malcolm H. Levitt, "Spin Dynamics: Basics of Nuclear Magnetic Resonance. 2nd ed," Wiley, 2008. 543.

[13] D. McRobbie *et al.*, "MRI: From Picture to Proton. 2nd ed," Cambridge, 2006. 148.

[14] Sam E. Day *et al.*, Nature Medicine **13**(11), 1382 (2007).

[15] C. R. Malloy, M. E. Merritt and A. D. Sherry, NMR Biomed. **24**, 973 (2011).

[16] Otto Warburg, Science **123**(3191), 309 (1956).

[17] M. J. Albers *et al.*, Cancer Res. **68**(20), 8607 (2008).

[18] Jan H. Ardenkjaer-Larsen *et al.*, NMR Biomed. **24**, 927 (2011).

[19] L. Lumata *et al.*, J. Phys. Chem. A **116**(21), 5129 (2012).